Title

Comparison of Manual and Automated Measurements of Tracheobronchial Airway Geometry in Three Balb/c Mice



Journal

The Anatomical Record, 300(11)

ISSN

1932-8486

Authors

Islam, Asef
Oldham, Michael J
Wexler, Anthony S

Publication Date

2017-11-01

DOI

10.1002/ar.23624

Peer reviewed

# Comparison of Manual and Automated Measurements of Tracheobronchial Airway Geometry in Three Balb/c Mice

**ASEF ISLAM**,[1] **MICHAEL J. OLDHAM**,[2] **AND ANTHONY S. WEXLER**[3]*
[1]Biomedical Engineering, Johns Hopkins University, Baltimore, Maryland 21218
[2]Altria Client Services, Richmond, VA 23103
[3]Mechanical and Aerospace Engineering, University of California, Davis, California

ABSTRACT

Mammalian lungs are comprised of large numbers of tracheobronchial airways that transition from the trachea to alveoli. Studies as wide ranging as pollutant deposition and lung development rely on accurate characterization of these airways. Advancements in CT imaging and the value of computational approaches in eliminating the burden of manual measurement are providing increased efficiency in obtaining this geometric data. In this study, we compare an automated method to a manual one for the first six generations of three Balb/c mouse lungs. We find good agreement between manual and automated methods and that much of the disagreement can be attributed to method precision. Using the automated method, we then provide anatomical data for the entire tracheobronchial airway tree from three Balb/C mice. Anat Rec, 300:2046–2057, 2017. © 2017 Wiley Periodicals, Inc.

**Key words: airway geometry; BALB/c mice; CT imaging; automated measurement**

## INTRODUCTION

Rodents are ubiquitous as model organisms. While the tracheobronchial structure of rats has been measured and involved in interspecies analysis (Raabe et al., 1976; Phalen and Oldham, 1983; Phillips and Kaye, 1995) and compared to humans (Hofmann et al., 1989), that of mice has been relatively absent from literature until recently. One reason for this is size, with the mouse lung being an order of magnitude smaller than the rat lung and several orders smaller than the human by volume (Irvin and Bates, 2003), making measurement of airways challenging. Since mice strains are predominantly employed as animal models in pulmonary toxicology studies, it is essential that tracheobronchial airway architecture is accurately described in order to model regional dose of toxins and therapeutics.

Recent advancements in imaging technology have allowed for high-resolution computed tomography, micro-CT, and magnetic resonance scans to be performed in-vivo and on lung casts. Furthermore, the data produced from these scans can be computationally processed to extract airway geometry more thoroughly and efficiently than is practically possible with manual measuring methods. A number of methods have been employed to extract airway geometry from scans including segmentation and skeletonization (Aykac et al., 2003; Chaturvedi and Lee, 2005; Carroll et al., 2006; Artaechevarria et al., 2009; Counter et al., 2013). In prior work, we have used such computational methods to quantify the airway tree by applying an airway bifurcation geometry model to CT scan data using a simulated annealing optimization process (Lee et al., 2008a; Lee and Wexler, 2011). We have used this approach extensively with rats, both in a

Additional Supporting Information may be found in the online version of this article.

*Correspondence to: Anthony Wexler, Mechanical and Aerospace Engineering, University of California, Davis, California. E-mail: aswexler@ucdavis.edu

Received 2 January 2017; Revised 11 March 2017;
Accepted 28 March 2017.
DOI 10.1002/ar.23624
Published online 20 June 2017 in Wiley Online Library (wileyonlinelibrary.com).

general structural characterization study (Lee et al., 2008b) and in studies on the effects of ozone and particle inhalation on postnatal airway development (Lee et al., 2010, 2011).

It follows naturally that this approach be utilized to address the complexity of characterizing mouse lung architecture. Previous studies with mice have reported measurements by generation, noted the monopodial structure as opposed to the symmetric dichotomous structure of human lungs, and considered implications to dosimetry and particle deposition (Oldham and Phalen, 2002; Oldham and Robinson, 2007; Madl et al., 2010; Moss and Oldham, 2011; Winkler-Heil and Hofmann, 2016). Studies have also discussed the use of micro-CT imaging in analyzing mouse airway structure (Thiesse et al., 2005; Thiesse et al., 2010). Other methods, such as photographic processing (Onuma et al., 2001) and MRI (Einstein et al., 2008; Oakes et al., 2012), have also been used on lung tissue and lung casts to extract geometry. This study had two goals: First, we aimed to assess how well manual and automated, computational measurement methods compare in the first six generations of the tracheobronchial airway of Balb/C mice, using the basic airway geometry parameters of branch diameter, length, and angle. Second, we sought to characterize the entire tracheobronchial airway tree, parameter uncertainties, and interanimal variability in Balb/C mice.

## MATERIALS AND METHODS

### Acquisition of Lung Casts

In order to obtain the data necessary for this study, casts were produced from the lungs of Balb/C mice. The mice were lethally injected with sodium pentobarbital. Their chests were then opened and lungs ventilated with carbon dioxide before being injected with silicone rubber to produce the cast. This casting procedure was described in detail in Madl et al. (2010), Oldham and Phalen (2002), Oldham and Robinson (2007), Oldham et al. (1994), and Phalen et al. (1973). These procedures were reviewed and approved by the IACUC at University of California, Irvine. Three lung casts produced in 2001 under this protocol were used in this study, referred to as Lungs 1, 2, and 3. Each came from male mice with body masses of 22.41 g, 24.4 g, and 25.92 g, respectively.

### Manual Lung Geometry Extraction

After lung casts were produced, manual airway measurements were made under a 10× magnifying lens (see Fig. 1, left and Supporting Information Tables S1–S3). Distances (branch diameter and length) were reported to the nearest 0.05 mm and angles to the nearest 5°, as described in prior work (Oldham and Phalen, 2002; Oldham and Robinson, 2007; Madl et al., 2010). These measurements, made in 2002, were incorporated in previous publications in the form of summary statistics, but never reported to the level of detail presented here. In order to estimate the precision of the manual measurements, the parameters of 5 random daughter airway pairs in all three lungs were remeasured. The remeasurements were made 14 years after the original measurements. These remeasurements are available in Supporting Information Table S4. The mean absolute value difference and standard deviation between the original and remeasured values were 0.032 (± 0.05) mm for diameter, 0.067 (±0.12) mm for length, and 6.6 (±12) degrees for branch angle.

### Automated Lung Geometry Extraction

After manual lung geometry extraction was completed, the lung casts were CT scanned by the Center for Molecular and Genomic Imaging at the University of California, Davis, on a commercially available MicroCAT II (Siemens, Knoxville, TN) at approximately 0.014 mm resolution. As was done in our prior work with rats (Lee et al., 2008b, 2010, 2011), some preprocessing steps were necessary to prepare the images for geometry extraction, described as follows, and outlined in Figure 2.

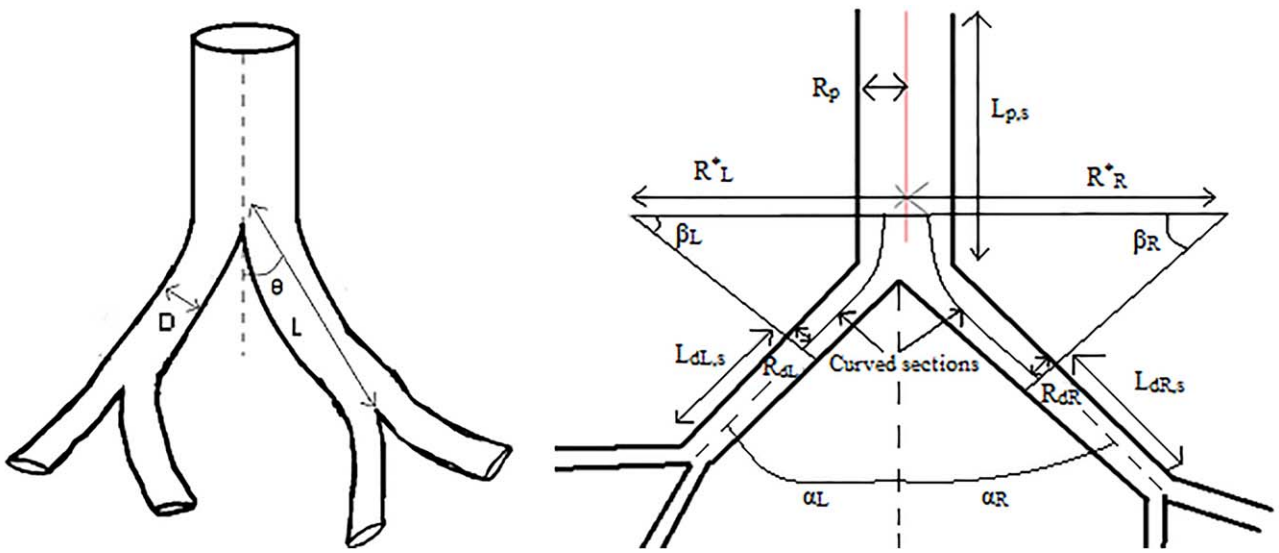


Fig. 1. Left- Diagram of parameter definitions ($D$ = Diameter, $L$ = Length, $\theta$ = Branch Angle). Right- Cross-sectional diagram of flexible bifurcation model (Parameters in text).

***Preprocessing.*** ImageJ was used to convert the 16 bit TIFF format files produced by the CT scanner to 16 bit signed raw format. The binary threshold tool within ImageJ was then used to color the airway lumen white and the rest of the image black. High contrast helps the geometry extraction software accurately process the images. Figure 3 shows the difference between prethreshold and postthreshold images.

***Bifurcation model.*** The simulated annealing (SA) optimization algorithm of Lee and coworkers (Lee et al., 2008a; Lee and Wexler, 2011) extracted tracheobronchial airway geometry from the preprocessed CT scan by minimizing the distance between a flexible bifurcation model and bifurcations present in the CT scans. This method, used in prior work to assess the lung architecture of Sprague Dawley rats (Lee et al., 2008b), revealed

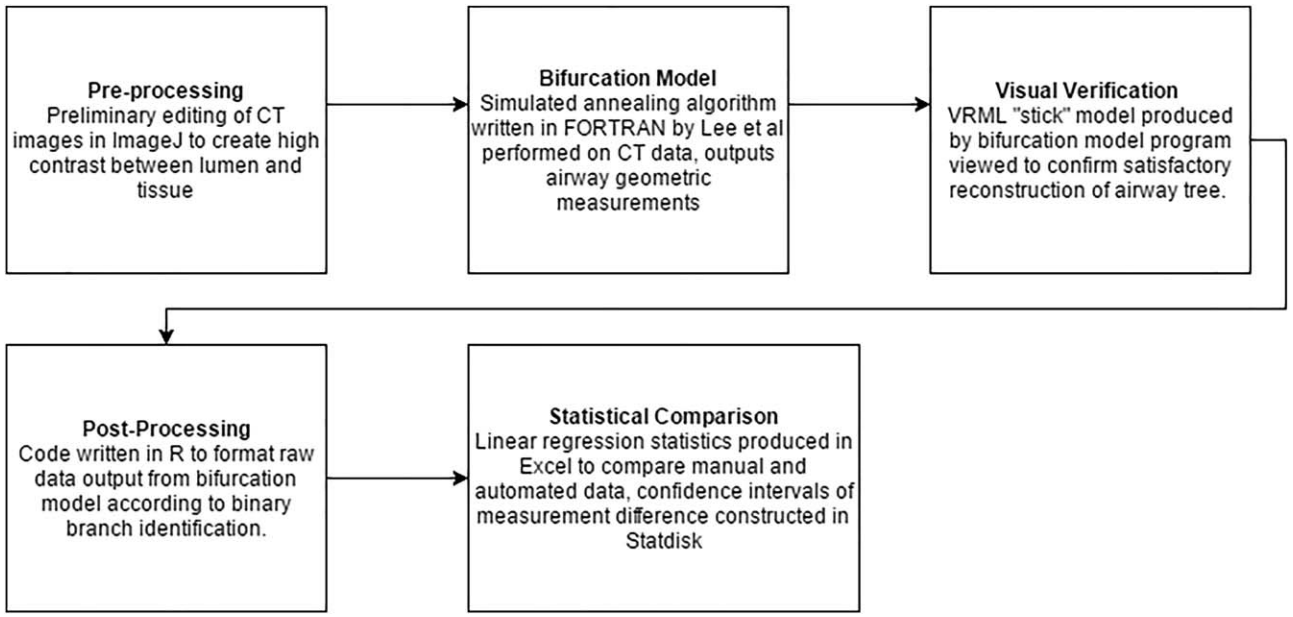


Fig. 2. Image processing and data comparison flowchart.

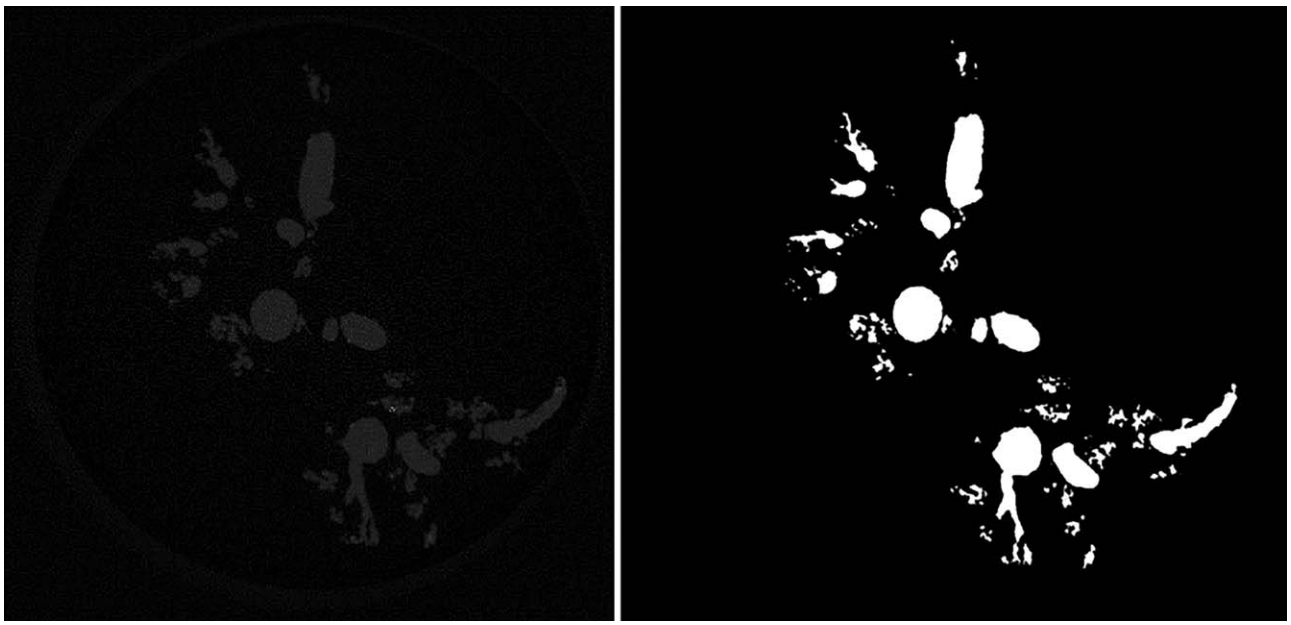

Fig. 3. Original CT scan image (left) vs. Thresholded CT scan image (right).

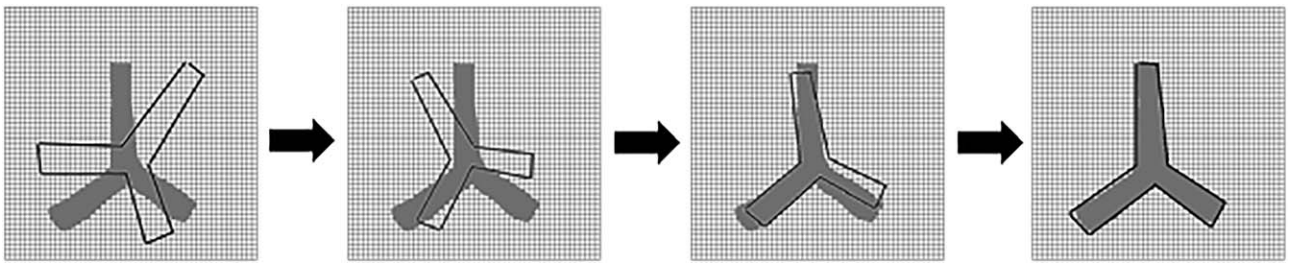

Fig. 4. Depiction of SA optimization process. Gray pixels indicate bifurcation in CT image, solid black lines represent outline of fitted bifurcation model.

disruptions in postnatal airway development due to inhalation of atmospheric pollutant particles and ozone (Lee et al., 2010, 2011). While full details regarding the underlying algorithms and equations of this modeling process are available in the cited papers, the following is a brief summary:

The structure of the mammalian lung begins with the initial bifurcation of the trachea into the two primary bronchi and subsequent bifurcations of these into continually smaller branches. Each bifurcation can be modeled by dividing it into the parent branch, the transition zone, and the two daughters, as depicted in Figure 1, right. This flexible model can be fitted to the CT scan data by optimizing the parameter values to minimize the distance between the model and CT image (Fig. 4). The software performs this optimization recursively from the trachea down the airway tree. The algorithm stops once the diameter of the airways becomes less than 5 voxels since error in geometry extraction values increases dramatically for smaller sizes that have insufficient image resolution.

The optimized parameters labeled on Figure 1, right, are:

- Radius of parent airway ($R_p$)
- Length of straight section of parent branch ($L_{p,s}$)
- Radii of daughter branches ($R_{di}$)
- Lengths of straight section of daughter airways ($L_{di,s}$)
- Subtended angles of daughter airways ($\beta_i$)
- Radii of curvature of the daughter airways ($R^*_i$)
- Angle of flow change from parent to daughter ($\alpha_i$)

These parameters were made comparable to the manual measurements as follows:

a. Diameter was found by doubling the radius.
b. Length for each branch was found by adding its straight section length to the length of the curved section between it and its parent. The length of the curved section was calculated by multiplying the radius of curvature by the subtended angle.
c. The angle of flow change is the same as the branching angle, $\alpha_i$.

The optimization process used an SA algorithm with shorter Markov chain length to search for parameter values that decreased the average distance between the fitted model and pixels of the CT images. When the distance between the CT image of the airway and the airway model was minimized, the SA process was terminated and the fit accepted. Figure 5 shows reconstructed airways from the CT scan and those from the SA extracted geometry.

***Postprocessing code.*** The bifurcation model is bifurcation oriented, as its name implies, in that it sequentially traverses the tracheobronchial airways identifying the geometry of each bifurcation as it progresses. The manual measurements are classified by branch, using the binary labeling format of Raabe and coworkers (Raabe et al., 1976). A postprocessing code written in R was used in order to convert the raw data produced by the bifurcation model into a formatted data table for ease in comparison to manual measurements of branches. In the raw data output, each branch and its associated geometric information is organized by integer branch numbers; the post processing code simply reclassifies this data into a table and constructs the binary identification labels for each branch for consistency with the method used to label branches manually. The resulting data for all three lungs are listed in Supporting Information Tables S1–S3.

## Comparison of Geometric Parameters

The binary branch identification system labels branches using sequences of 1s and 2s. The trachea is identified as 1, and the label of every daughter is equivalent to the label of the parent with either a 1 or a 2 added to the sequence, a 1 indicating the major daughter (larger diameter) and a 2 indicating the minor daughter. Corresponding branches in the manual record and automated results were matched up by binary branch identification number, and the geometric information was compared.

The parameters compared were diameter, length, and branch angle (defined as the angle of change in flow direction from parent to daughter, measured using a centerline approach). In addition to the branch length, the cumulative length down the tree at the end of each branch was also calculated to minimize differences in identification of starting/ending positions of each branch.

The cumulative length for each branch is defined as the sum of its length and the lengths of all parents preceding it, up to the end of the trachea. Comparison of this value between the automated and manual measurement of length should be more similar than the length comparison itself because cumulative length reduces differences due to different definitions between the automated and manual methods of starting and ending position.

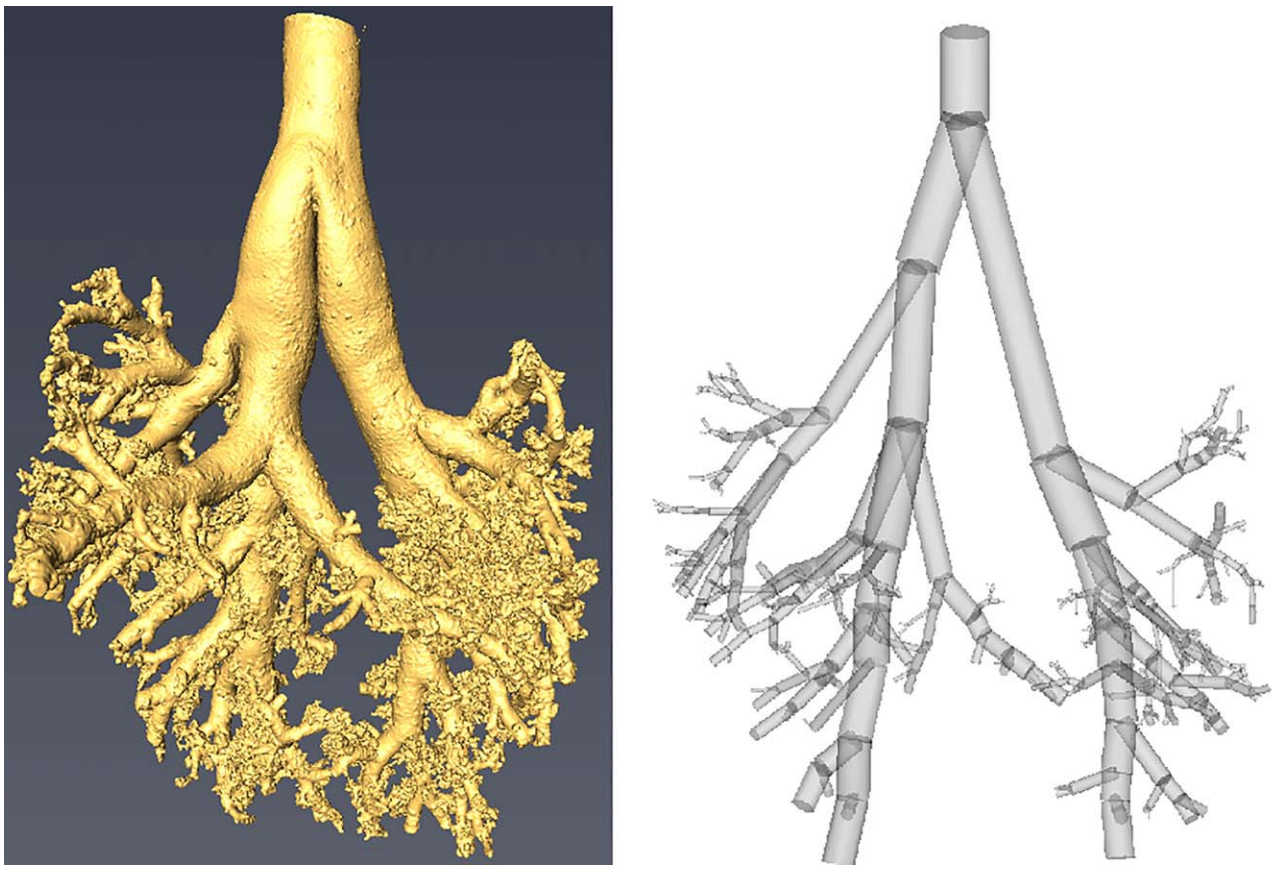

Fig. 5. Comparison between a 3D rendering of the CT scan images created using Amira (left) and a "stick model" depiction of the airway tree produced by the postprocessing code (right). The stick model is not intended as an accurate representation of the airways, but rather as a visualization of the extracted geometry to check that the code found all the relevant airways. The stick model also doubles airway length compared to airway diameter to spread out airways and help with visualization.

Occasionally there will exist what appears to be a "trifurcation" in the tree, where the parent branch will essentially split into three daughters rather than just two. While the automated data output literally represents this as three daughters from one parent, in the manual method this is represented as two subsequent bifurcations, where the intermediate branch is assigned a length of 0.1 mm and branching angle of 0°. There were two to four of these cases in each lung. The branch identification of the automated results was corrected to match the manual for these trifurcation cases.

### Software Usage Procedure

Figure 2 illustrates the steps of the computational data extraction and result comparison process, with the software used in each.

## RESULTS

The complete set of parameter measurements for the first 6 generations of each lung is included in Supporting Information Tables S1–S3. Figure 6 compares parameter values produced by the manual and automated measurements. The slope, $m$, and correlation coefficient, $r$, of a straight line fit to the data, with the intercept forced through (0,0) indicated goodness of fit. The histograms in Figure 7 show the bias in the measurement comparisons.

Table 1 shows 95% confidence intervals for the predicted population mean differences between the two methods for each parameter for each lung, calculated using the $t$-test algorithm within Statdisk (© Triola and Pearson 1986–2013).

The question now arises as to the source of the differences between the methods. In order to estimate the portion of the differences due to precision, both measurements were repeated. Dimensions were manually remeasured in some of the airways. To accomplish the same for the automated method, the model was rerun on each lung using a different starting position in the trachea, thus causing it to take a different route while traversing down the airway tree and replicating the results for determination of precision (Supporting Information Table S5). Figure 8 shows BA plots (Bland and Altman, 1986) of the differences between original and remeasured values for each parameter for both methods.

We attributed the precision for each measurement to be ± two standard deviations of the differences between original and remeasured values, thus giving the limits of error with approximately 95% confidence. These margins

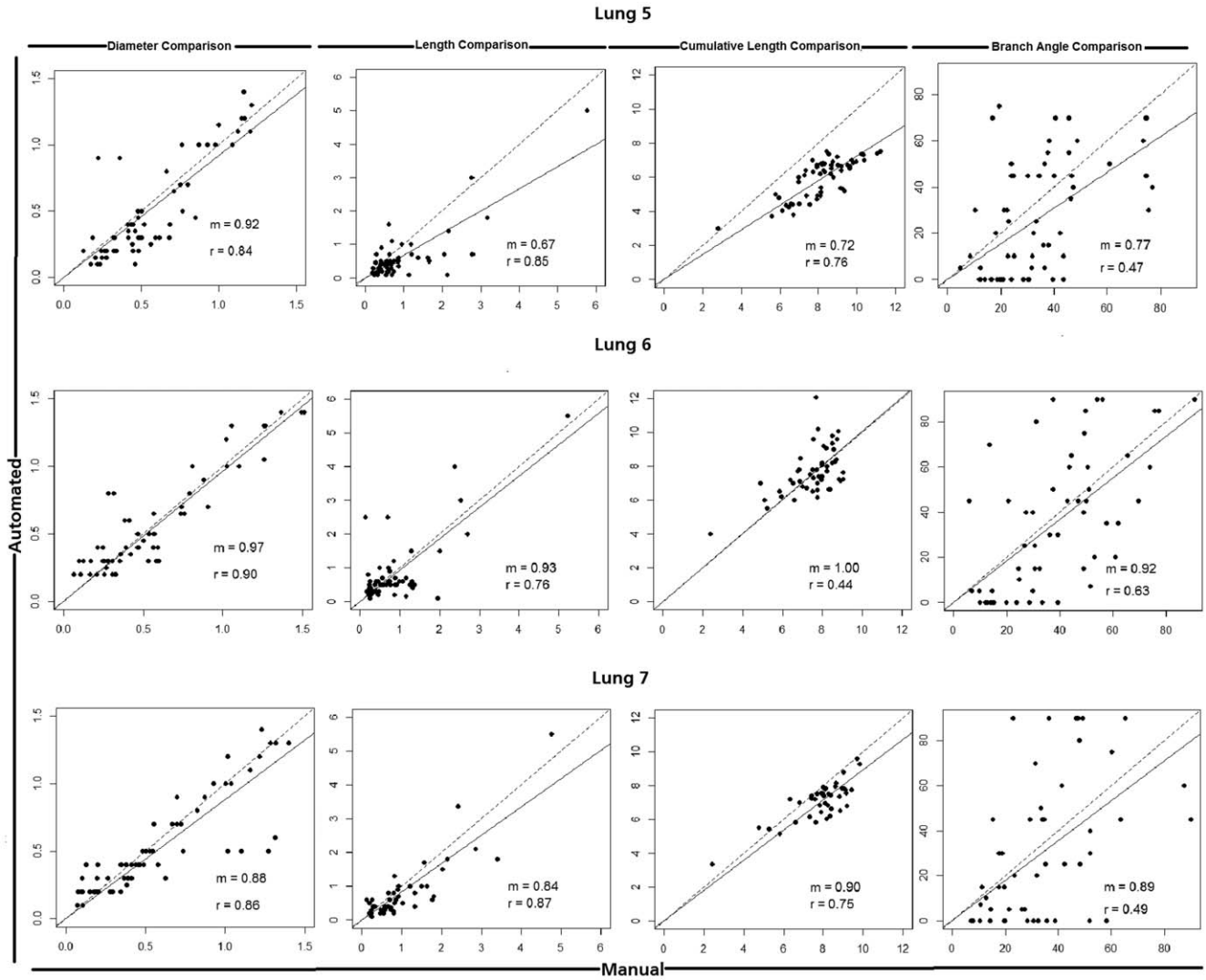


Fig. 6. Comparison between automated and manual measurements of diameter, length, cumulative length and branch angle using a linear regression analysis. The solid line represents the best-fit, and the dashed line $y = x$.

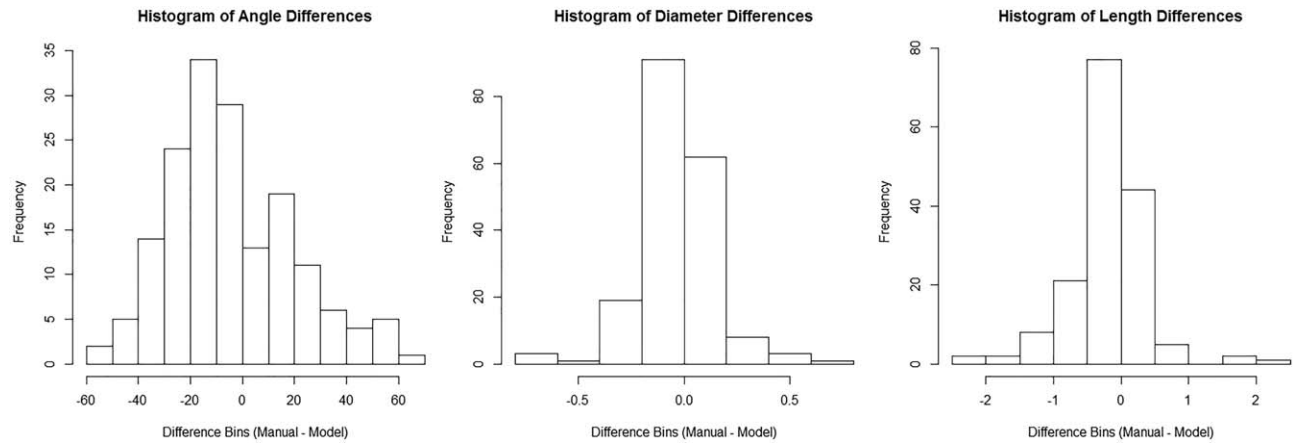


Fig. 7. Histograms showing the frequency distribution of error for each parameter, illustrating the degree of bias in the comparison.

**TABLE 1. Confidence intervals for measurement differences (manual – automated)**

| Lung | Diameter | Length | Cumulative length | Branch angle |
|---|---|---|---|---|
| 1 | $-0.11 < \mu d < -0.01$ | $-0.43 < \mu d < -0.15$ | $-2.46 < \mu d < -1.98$ | $-12.31 < \mu d < -0.77$ |
| 2 | $-0.04 < \mu d < 0.04$ | $-0.20 < \mu d < 0.15$ | $-0.21 < \mu d < 0.47$ | $-9.67 < \mu d < 2.99$ |
| 3 | $-0.09 < \mu d < 0.01$ | $-0.35 < \mu d < -0.08$ | $-1.02 < \mu d < -0.52$ | $-10.31 < \mu d < 5.03$ |

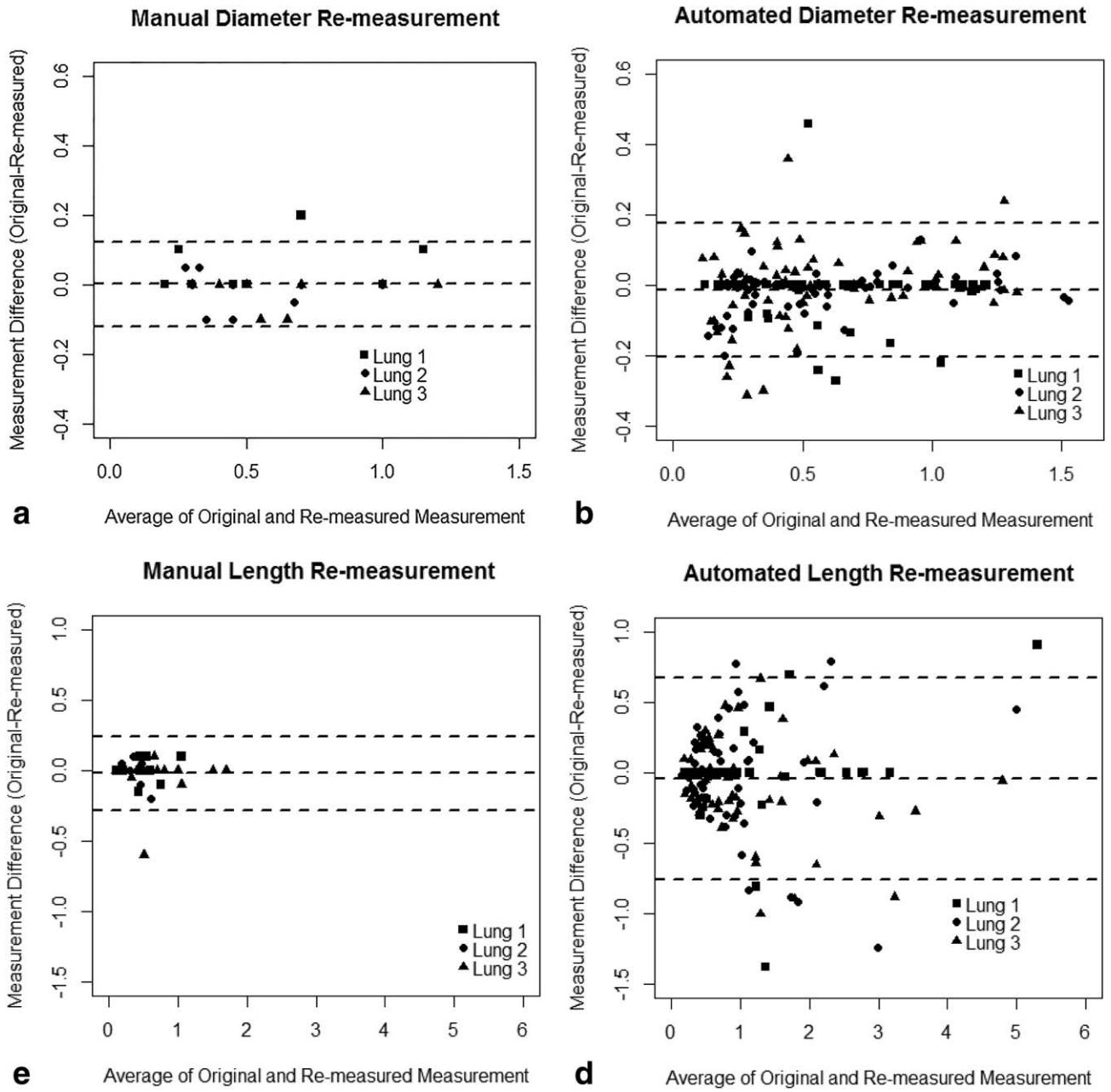


Fig. 8. Bland Altman (BA) plots comparing sets of measurements by plotting the difference between the two measurements as a function of the average of the two. Three dashed lines are also inserted, with the middle being the mean of the differences and the outside two showing two standard deviations from the mean. (a) Manual diameter remeasurement differences, (b) Automated diameter remeasurement differences, (c) Manual length remeasurement differences, (d) Automated length remeasurement differences, (e) Manual branch angle remeasurement differences, (f) Automated branch angle remeasurement differences.

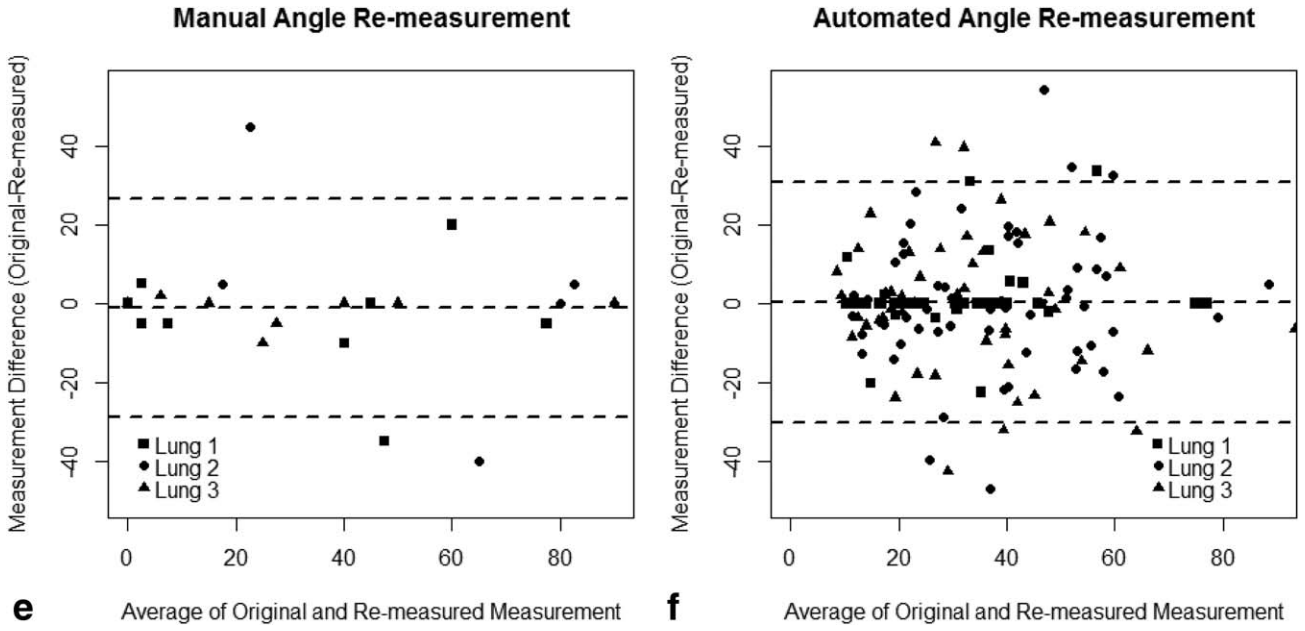


Fig. 8. (Continued).

**TABLE 2. Estimated measurement precisions**

| Parameter | Manual precision | Automated precision | Combined precision |
|---|---|---|---|
| Diameter (mm) | ± 0.12 | ± 0.19 | ± 0.31 |
| Length (mm) | ± 0.26 | ± 0.72 | ± 0.98 |
| Angle (Degrees) | ± 27 | ± 31 | ± 58 |

are given in Table 2. Remeasurement data for both methods are given in Supporting Information Tables S4 and S5.

Figure 9 shows BA plots of the relative difference between methods. Bland and Altman (1986) argued that correlation does not necessarily imply agreement when comparing two methods of measurement, thus these provide a further analysis of the level of agreement beyond the scatterplots while also accounting for method precision.

## DISCUSSION

We observed a generally strong correlation (avg. 0.86) and best-fit slope near 1 (avg. 0.92) in the diameter comparisons across all three lungs, indicating a relatively high agreement in both the measurement of the diameters and branch identification (Fig. 6). Bland-Altman plots and error histograms show that most of the diameter errors lie within a reasonable margin from 0, with the histogram showing that the vast majority (approximately 80%) are within 0.2 mm (Figs. 7 and 9a,b). Additionally, the 95% confidence intervals for the expected population means reveal some peculiar differences between the three lungs (Table 1). The interval for diameter in Lung 2 is centered almost exactly about 0, with a 0.04 mm margin in either direction. However, for both Lungs 1 and 3, the interval is negative, with a mean difference of up to 0.1 mm. This implies that the manual measurements are consistently smaller than those produced by the automated method. Nearly the same disparity exists between the lungs in the length measurements. However, this potential bias was seen only in two of the three lungs.

There was also a strong correlation in the length comparison (avg. 0.81) and average best-fit slope of 0.81. However, the large lengths of the main bronchi had a significant effect on the overall statistics. When the comparison was restricted to airway lengths <2 mm measured by both methods, the average correlation coefficient was reduced to 0.44. The Bland-Altman plot shows the majority of the differences being near 0 when the average of the manual and automated method length is less than 1 mm. Differences are larger for lengths greater than 1 mm. The histogram also shows a large majority of the errors to be within 0.5 mm in either direction. Again, we would have ideally hoped for the margin of differences to be relatively smaller. However, some further confidence was provided by the cumulative length comparison, with an average slope of 0.88 and correlation of 0.65, that the total length of airways measured down the tree remains relatively similar through the six generations. For this to be true, it was predicted that the cumulative length should be closer to the 1:1 line, and it appears to do so reasonably well based on the scatterplot.

A large proportion of the imprecision in the manual measurements, especially in diameter and small lengths, could simply be due to rounding, as these measurements are reported to the nearest 0.05 mm. Additionally, due to the 14-year time span between the initial manual measurements and the manual remeasurements, estimates of precision also include measures of the temporal

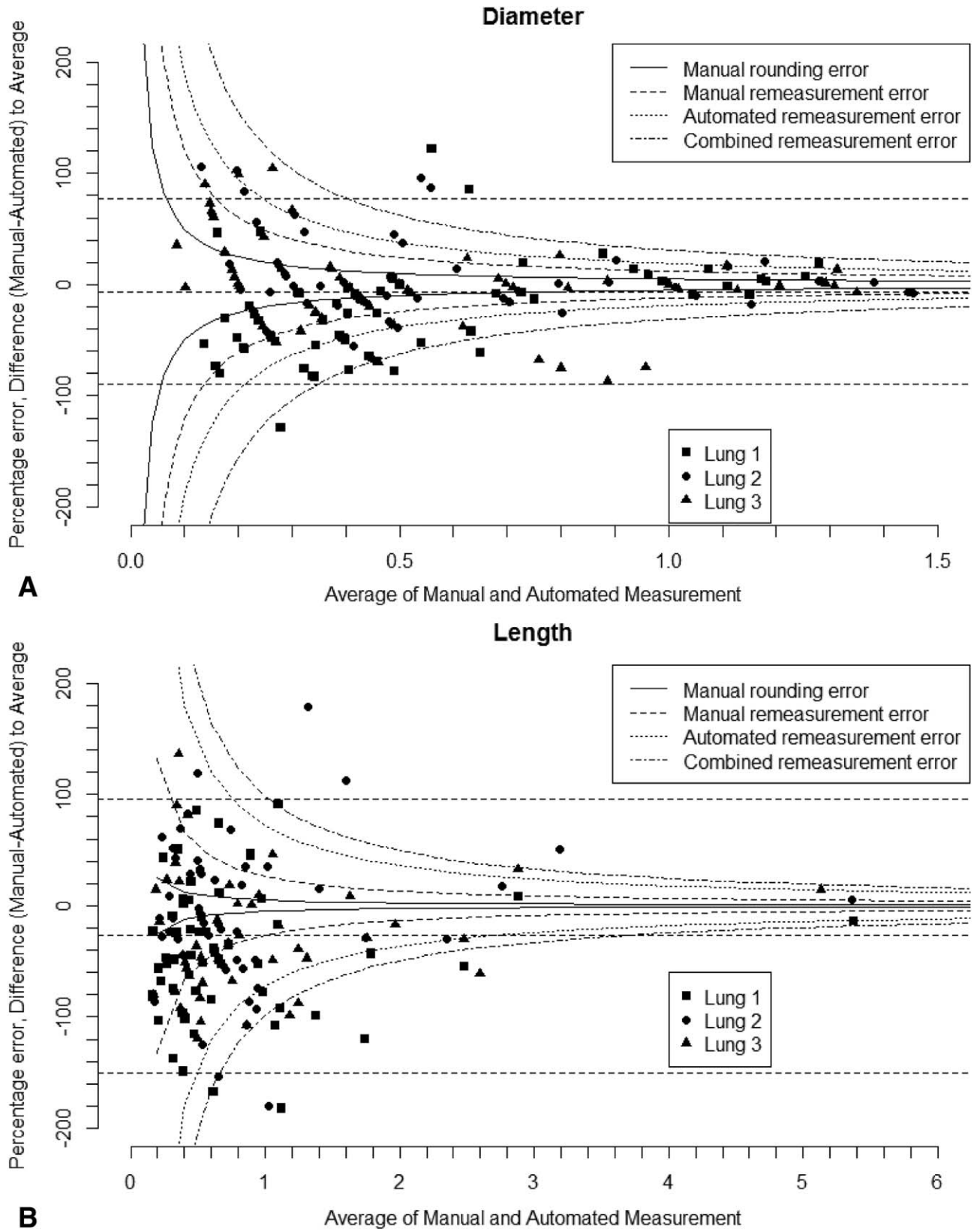


Fig. 9. Relative BA plots comparing methods for each parameter. Curved lines show the precision for each method and the combined precision of both methods. Again, dashed straight lines show the mean (central line) and two standard deviations about the mean. There are several branches for which the angle percent error is 200%, which correspond to a manual value of 0. (a) Diameter BA plot, (b) Length BA plot, (c) Branch Angle BA plot.

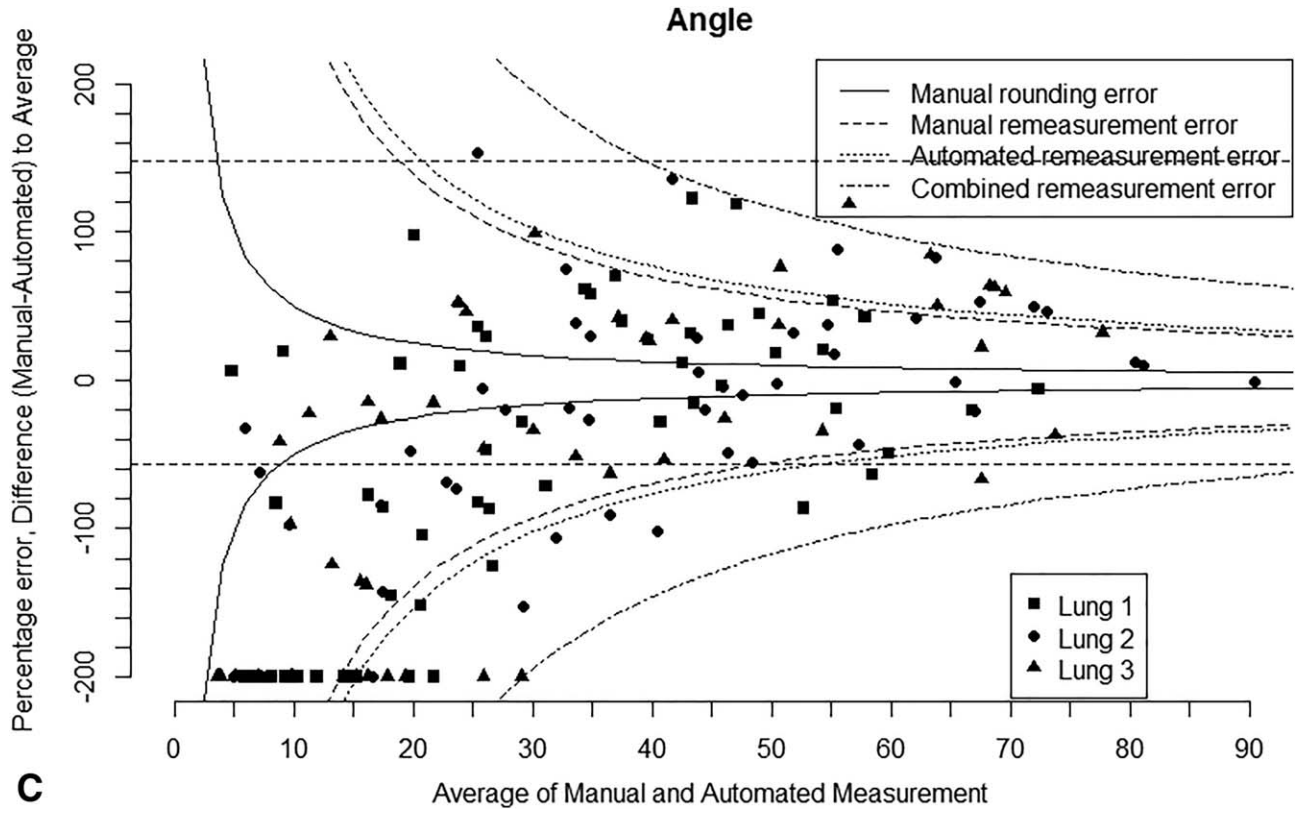


Fig. 9. (Continued).

stability of the casts. The remeasurement data showed that in the diameter measurements both methods had a similar and reasonably small imprecision, however in length, the automated method actually appears to be much less precise than the manual measurements.

There is also a slight difference in the fundamental definitions of length for each method, which were described in the methods section. The automated method defines total length by measuring the straight section of the branch and adding the arc length of the curved transition region from its parent. However, in the manual method, a single straight length is measured from one bifurcation to the next, without assuming any curvature. This distinction adds a small amount of error to all length comparisons.

Perhaps the most important insight was given by the relative BA plots (Fig. 9) with consideration of the amount of intermethod comparison error attributable to the intrinsic measurement error of each method, estimated using the difference margins of the remeasured values. For all three parameters, more than 90% of the data fit within the curves representing the potential combined measurement error of both methods, suggesting that the data agrees within the limits of precision for each method. It also reveals, especially for diameter and length, that there is a clear trend of decreasing relative error as the parameter value increases. Logically, as the value of the parameter increases, there will be less of an effect in terms of relative error made by the constant amount of measurement imprecision that is present in each method. In the manual method this is likely caused by rounding, whereas in the automated method is likely caused by the voxel size. Thus, increasing the level of precision in each method should decrease the amount of error in the intermethod comparisons, such as by using more precise measuring instruments in the manual method or higher-resolution CT scans for the automated method.

Diameter and length values alone allow for numerous analyses of lung architecture, such as those seen in both mice (Madl et al., 2010) and rats (Lee et al., 2008b). These include observing the relationships between lengths and diameters with termination probabilities, as well as length/diameter ratios and parent/daughter ratios. These parameters have been extensively reported (Phalen and Oldham, 1983; Oldham et al., 1994; Oldham and Robinson, 2007; Moss and Oldham., 2011). The data in Oldham and Robinson (2007) includes the manual measurements used in this study in addition to manual measurements from other in-situ prepared Balb/c mouse casts. Figure 10 compares the averages through six generations reported by Oldham and Robinson (2007) to those from the data in this study, for both the manual measurements and the automated ones. In general, all of the progressions of the averages through generations seem to conform well for both parameters, however, it appears that there is about as much intraspecies variation as there is intermethod variation among the lungs

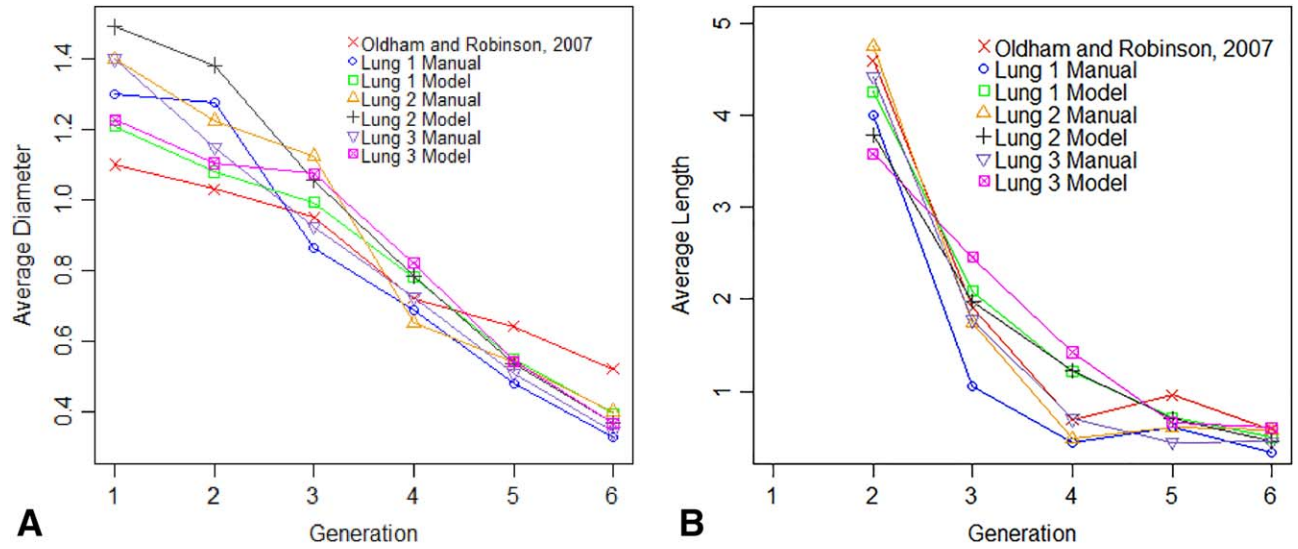


Fig. 10. (a) Generational averaged diameter. (b) Generational averaged length.

in this study. Nevertheless, this study was the first attempt to compare automated parameter measurements to manual measurements on a branch by branch basis, in addition to being the first time that these automated methods were applied to the mouse lung.

While the reasonably high level of coincidence in diameter and length values is encouraging, the same cannot be said of the branching angles. Although the average slope of the branch angle comparison is 0.86, the correlation coefficient is only 0.53. In addition, the Bland-Altman plot shows a wide spread of error throughout the entire range of angle values. We speculate that the high error present in both the manual and automated branch angle measurements may be due in part to the small lengths of many of these airways. This may present difficulty in the placement of centerlines to measure branching angles in both methods. As seen in Figure 11, there is a much greater probability of having a high difference when the length is below 1 mm. For lengths above 2 mm, most differences are within 20°. More data would be necessary to test this claim further. Another possible source of precision error within the manual angle measurements is that the positioning of the bifurcation needed to measure the angle often involves moving the airway to obtain the necessary view, which may distort the angle in the process. The remeasurements revealed a rather high level of error in the manual angles, with a standard deviation of differences of about 10°, and a few outliers of very large differences between the originally measured and remeasured angles.

Another factor that has potential for contributing to error in all three parameters is the possibility of differences in branch identification between both methods. Because the distinction between minor and major daughters depends solely on diameter, pairs of daughters that have nearly equal diameter values could be identified differently. Thus this would not produce a clear impact on the diameter comparison within that generation, but it could affect the other two parameters. In addition, in any instance in which this occurs, all subsequent daughters down the remainder of the tree will also be identified differently. However, after performing a manual authentication of the airway identifications of the automated method by matching branches based on diameters and lengths to those reported manually, few misidentifications occurred limiting the effect on estimated error.

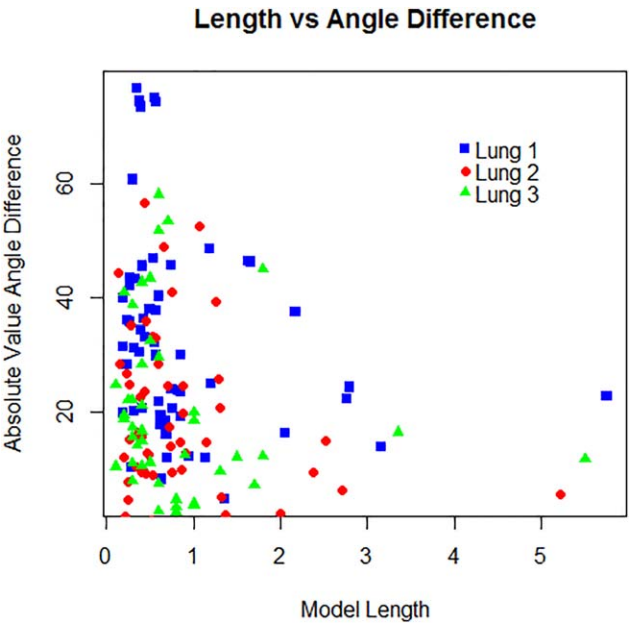


Fig. 11. Effect of length on angle difference.

In terms of the application to toxicology studies, diameter- and length-based analyses can prove useful in providing many findings, such as disruption of airway growth and estimating local dose. However, more accurate branch angle information would enable more robust deposition and flow modeling.

The comparisons presented here were limited to the first six generations of the tracheobronchial airway tree, as a first comparison of automated and manual measurement methods. The automated method analyzed the entire tracheobronchial airway tree, but the data are too voluminous to include here. These data can be obtained by contacting the authors.

## CONCLUSION

The manual and automated measures of diameter and length agreed reasonably well. Most of the disagreement that does exist between the methods was attributed to each method's inherent measurement errors—its precision. These measurement results were similar, based on generational average, to previously reported measurements in mouse lungs. However, agreement between branch angle measurements between the methods was less robust, which was attributed to the short length of the airways and the concomitant uncertainty in the centerline direction of each parent and daughter airway.

## LITERATURE CITED


Artaechevarria X, Munoz-Barrutia A, van Ginneken B, Ortiz-de-Solórzano C. Fast murine airway segmentation and reconstruction in micro-CT images. in 72620B–72620B (International Society for Optics and Photonics, 2009).

Aykac D, Hoffman EA, McLennan G, Reinhardt JM. 2003. Segmentation and analysis of the human airway tree from three-dimensional X-ray CT images. IEEE Trans Med Imaging 22:940–950.

Bland JM, Altman DG. 1986. Statistical methods for assessing agreement between two methods of clinical measurement. Lancet 327:307–310.

Carroll JRD, Chandra A, Jones AS, Berend N, Magnussen JS, King GG. 2006. Airway dimensions measured from micro-computed tomography and high-resolution computed tomography. Eur Respir J 28:712–720.

Chaturvedi A, Lee Z. 2005. Three-dimensional segmentation and skeletonization to build an airway tree data structure for small animals. Phys Med Biol 50:1405–1419.

Counter WB, Wang IQ, Farncombe TH, Labiris NR. 2013. Airway and pulmonary vascular measurements using contrast-enhanced micro-CT in rodents. Am J Physiol Lung Cell Mol Physiol 304: L831–L843.

Einstein DR, Neradilak B, Pollisar N, Minard KR, Wallis C, Fanucchi M, Carson JP, Kuprat AP, Kabilan S, Jacob RE, et al. 2008. An automated self-similarity analysis of the pulmonary tree of the Sprague-Dawley rat. Anat Rec Hoboken NJ 291:1628–1648.

Hofmann W, Koblinger L, Martonen TB. 1989. Structural differences between human and rat lungs: implications for Monte Carlo modeling of aerosol deposition. Health Phys 57: 41–46. discussion 46–47.

Irvin CG, Bates JHT. 2003. Measuring the lung function in the mouse: the challenge of size. Respir Res 4:4.

Lee DY, Park SS, Ban-Weiss GA, Fanucchi MV, Plopper CG, Wexler AS. 2008a. Bifurcation Model for Characterization of Pulmonary Architecture. Anat Rec 291:379–389.

Lee DY, Fanucchi MV, Plopper CG, Fung J, Wexler AS. 2008b. Pulmonary architecture in the tracheobronchial regions of six rats. Anat Rec 291:916–926.

Lee DY, Wallis C, Wexler AS, Schelegle ES, Van Winkle LS, Plopper CG, Fanucchi MV, Kumfer B, Kennedy IM, Chan JKW. 2010. Small Particles disrupt postnatal airway development. J Appl Physiol 109:1115–1124.

Lee DY, Wexler AS. 2011. Simulated annealing implementation with shorter Markov chain length to reduce computational burden and its application to the analysis of pulmonary airway architecture. Comp Bio Med 41:707–715.

Lee DY, Wallis C, Van Winkle LS, Wexler AS. 2011. Disruption of tracheobronchial airway growth following postnatal exposure to ozone and ultrafine particles. Inhal Toxicol 23:520–531.

Madl P, Hofmann W, Oldham M, Asgharian B. 2010. Stochastic morphometric model of the BALb/c mouse lung. Anat Rec (Hoboken) 293:1766–1775.

Moss OR, Oldham MJ. 2011. Predicting Balb/c and B6C3F1 mouse sensitivity to inhaled methacholine: Impact of calculating lung-airway dimension and airflow distribution. Aerosol Sci Technol 45:821–826.

Oakes JM, Scadeng M, Breen EC, Marsden AL, Darquenne C. 2012. Rat airway morphometry measured from in situ MRI-based geometric models. J Appl Physiol Bethesda MD 112:1921–1931.

Oldham MJ, Phalen RF, Schum GM, Daniels DS. 1994. Predicted nasal and tracheobronchial particle deposition efficiencies for the mouse. Ann Occup Hyg 38:135–141.

Oldham MJ, Phalen RF. 2002. Dosimetry implications of upper tracheobronchial airway anatomy in two mouse varieties. Anat Rec 268:59–65.

Oldham MJ, Robinson RJ. 2007. Predicted tracheobronchial and pulmonary deposition in a murine asthma model. Pulmonary Bio 290:1309–1314.

Onuma K, Ebina M, Takahashi T, Nukiwa T. 2001. Irregularity of airway branching in a mouse bronchial tree: a 3-D morphometric study. Tohoku J Exp Med 194:157–164.

Phalen RF, Yeh HC, Raabe OG, Velasquez DJ. 1973. Casting the lungs in situ. Anat Rec 177:255–263.

Phalen RF, Yeh HC, Schum GM, Raabe OG. 1973. Application of an idealized model to morphometry of the mammalian tracheobronchial tree. Anat Rec 190:167–176.

Phalen RF, Oldham MJ. 1983. Tracheobronchial airway structure as revealed by casting techniques. Am Rev Respir Dis 128:S1–S4.

Phillips CG, Kaye SR. 1995. Diameter-based analysis of the branching geometry of four mammalian bronchial trees. Respir Physiol 102:303–316.

Raabe OG, Yeh HC, Schum GM, Phalen RF. 1976. Tracheobronchial Geometry: Human, Dog, Rat, Hamster. LF-53, UC-48, Inhalation Toxicology Research Institute, Lovelace Foundation for Medical Education and Research.

Thiesse J, Reinhardt JM, de Ryk J, Namati E, Leinen J, Recheis WA, Hoffman EA, McLennan G. 2005. Three-dimensional visual truth of the normal airway tree for use as a quantitative comparison to micro-CT reconstructions. *Proc. SPIE* 5746, Medical Imaging 2005: Physiology, Function, and Structure from Medical Images, 50.

Thiesse J, Namati E, Sieren JC, Smith AR, Reinhardt JM, Hoffman EA, McLennan G. 2010. Lung structure phenotype variation in inbred mouse strains revealed through in vivo micro-CT imaging. J Appl Physio 109:1960–1968.

Winkler-Heil R, Hofmann W. 2016. Modeling Particle Deposition in the Balb/c mouse respiratory tract. Inhal Toxicol 28:180–191.